Version of Record: https://www.sciencedirect.com/science/article/pii/S0150986119302020
Manuscript_f64157d01e7073e2b8ce87e1f3bba94b

# Comparison between MRI-derived ADC maps and $^{18}$FLT-PET in pre-operative glioblastoma

David Hassanein Berro[a,b], Solène Collet[c], Jean-Marc Constans[b,c], Louisa Barré[d], Jean-Michel Derlon[a,b], Evelyne Emery[a,e], Jean-Sébastien Guillamo[b,f], Samuel Valable[b]

[a] Department of Neurosurgery, University Hospital of Caen, Caen, France
[b] Normandie Univ, UNICAEN, CEA, CNRS, ISTCT/CERVOxy group, GIP CYCERON, Caen, France
[c] Department of Neuroradiology, University Hospital of Caen, Caen, France
[d] Normandie Univ, UNICAEN, CEA, CNRS, ISTCT/LDM-TEP group, Caen, France
[e] Normandie Univ, UNICAEN, INSERM, Inserm UMR-S U919, Caen, France
[f] Department of Neurology, University Hospital of Caen, Caen, France

Corresponding author: David H Berro
Service de neurochirurgie
CHU de Caen Normandie
Avenue de la Côte de Nacre
14000 Caen, France
Phone: 33 6 44 66 44 06
FAX: 33 2 31 06 45 99
dh@berro.net

© 2019 published by Elsevier. This manuscript is made available under the CC BY NC user license
https://creativecommons.org/licenses/by-nc/4.0/

# Comparison between MRI-derived ADC maps and $^{18}$FLT-PET in pre-operative glioblastoma

## ABSTRACT

*Background and purpose.* Among principal MRI sequences used for a better pre-therapeutic characterization of glioblastoma (GBM), DWI-derived ADC is expected to be a good parameter for the evaluation of cellularity, due to restricted water diffusivity. We aimed here to compare ADC maps to $^{18}$FLT-PET, a proliferation tracer, in GBM cases.

*Materials and methods.* Patients underwent $^{18}$FLT-PET, followed by multiparametric magnetic resonance imaging (MRI) just prior to surgery. We analysed in this study twenty GBM confirmed patients. The 5$^{th}$ percentile (5p) of the ADC values were thresholded to define the $ADC_{min}$ ROI, while the 95$^{th}$ percentile (95p) of the SUV FLT values were used to define the $FLT_{max}$ ROI. The statistical and spatial correlations between these two groups of ROIs were analyzed.

*Results.* We did not observe any significant correlations between $ADC_{min}$ and $FLT_{max}$ cut-off values ($R^2$ = 0.0285), neither between $ADC_{min}$ and $FLT_{max}$ ROIs (mean Dice = 0.09 ± 0.12). Mean ADC values in the $FLT_{max}$ defined ROI were significantly higher than the values in the $ADC_{min}$ ROI ($p < 0.001$). Mean FLT values in the $FLT_{max}$ ROI were significantly higher than the values in the $ADC_{min}$ ROI ($p < 0.001$).

*Conclusions.* When comparing ADC maps to $^{18}$FLT uptake, we did not observe significant anatomical overlap nor correlation, between the regions of low ADC and high FLT disabling to clearly link ADC values to cellular proliferation. The exact significance of ADC maps in GBM has yet to be elaborated.

**Keywords:** Glioblastoma; MRI; ADC; $^{18}$FLT-PET; Cellularity

## Introduction

Glioblastoma (GBM) is the most common primary brain tumor and one of the most aggressive forms of cancer in humans [1]. GBM is particularly resistant to antitumor treatments and is characterized by a high rate of rapid recurrence and a short survival (12-15 months) [2,3]. Patient management may benefit from a better pre-therapeutic characterization of the tumor [4], and advanced functional MRI sequences have been developed for further characterization of the tumor and extent, but have yet to be validated. Among them, diffusion-weighted MRI and the resulting apparent diffusion coefficient (ADC) is a sequence that has found its place in the management of many pathologies, such as acute ischemic stroke [5–7]. However, while routinely being used in glial tumors, its biological significance remains controversial [8]. Several studies have attempted to determine the role of ADC in gliomas, but with contradictory results. Some suggested that ADC can play a valuable role in the definition of the boundaries of malignant gliomas, between a low ADC due to increased cellularity and a high ADC due to the presence of vasogenic edema [9,10], whereas others failed to demonstrate the utility of ADC in delimiting the boundaries in gliomas [11–13]. It is mostly believed that cellularity is inversely correlated to the ADC [14]. Several studies succeeded to find a significant correlation between cellularity and the minimum ADC ($ADC_{min}$) in various types of brain tumors [4,15–17]. Higano et al. have shown a significant negative correlation between the minimum ADC and the proliferation index Ki-67 when analyzing anaplastic astrocytomas and GBMs together (i.e. malignant astrocytic tumors), but not when analyzing GBMs alone [18]. More recently, in a study performed on glioma patients with various grades, multiple MRI parameters were compared to Ki67 staining. Diffusion parameters were not among the best predictors, questioning the ability of diffusion MRI to predict tumor cell proliferation [19].

PET is of great interest to gain access to more functional and quantitative characterization of the tumor. The thymidine analog $^{18}$F-fluoro-L-thymidine ($^{18}$FLT) has been proposed as a biomarker of proliferation based on its relationship with thymidine kinase-1 (TK-1) and with cell proliferation [20,21]. Several studies have shown the utility of $^{18}$FLT-PET in glioma grading mainly by assessing the proliferation activity of tumors in vivo, particularly in brain tumors [21–25].

To date, $^{18}$FLT-PET, like other radiotracers PET examinations, is not routinely performed and ADC-MRI has appeared to be a well-suited examination for assessing cellular

density. While the ADC was recently shown to be correlated to $^{18}$FDG [26], Rose et al. [27] failed to correlate the $ADC_{min}$ to $^{18}$F-Fluoro-L-DOPA, another reliable proliferation index.

In this study, we aimed to analyze the correlation between the ADC and FLT, especially between their most significant and clinically relevant extreme areas, namely, the minimum ADC ($ADC_{min}$) and maximum FLT ($FLT_{max}$). This study was performed in 20 GBM confirmed patients.

## Materials and methods

*Patient Population*

This study was based on a prospective clinical trial funded by INCa (Institut National du Cancer) and approved by the local ethics committee and AFSSAPS agreement (ClinicalTrials.gov identifier: NCT00850278). In this trial, twenty patients from the Caen University Hospital were included. The inclusion criteria were as follows: a presumed diffuse glioma amenable to surgical resection or biopsy, an age greater than or equal to 18 years, a Karnofsky Performance Status (KPS) greater than or equal to 50, a normal blood cell count, normal biological hepatic functions and a signed informed consent. Only confirmed cases of GBM were considered in our study. The patients first underwent $^{18}$FLT-PET, followed by multiparametric MRI within the same week and prior to surgery. Thereafter, patients underwent surgery, resection or biopsy depending on the location of the tumor, and the specimens were histopathologically evaluated by an experienced neuropathologist.

*Image Acquisition*

MRI was performed on a 1.5 Tesla GEMS version HDXt 15.0. After scout-view, T2 and FLAIR imaging, DWI was performed using spin-echo-echo planar imaging (SE-EPI) (3 diffusion directions, 36 slices, slice spacing: 7 mm resulting in a voxel resolution: 1.09 × 1.09 × 7 mm, TR/TE = 6000/96 ms, b ≈ 0 and b ≈ 1000 s/mm$^{-2}$). A 3D T1WI sequence after gadolinium injection (3DT1w-Gd) (124 slices, slice spacing: 1.5 mm, pixel resolution: 1.01 mm × 1.01 mm, and TR/TE = 17/3 ms) was performed. T2Star gradient echo weighted images (pixel resolution: 1.8 × 1.8 mm, slice thickness: 5 mm, TR/TE = 1120/31.9 msec) were also performed to assess hemorrhages.

$^{18}$FLT was produced by the LDM-TEP group as described by Jacobs et al. [25]. Acquisitions were performed on a General Electric Discovery VCT 64 PET scanner, slice spacing was 3.2 mm. Images of the brain were acquired 40 min after the intravenous

injection of 5 MBq/kg of $^{18}$FLT and lasted for 20 min. The attenuation-corrected images were reconstructed with an OSEM 2D algorithm and filtered in 3D with a Butterworth filter (9 subsets and 2 iterations).

*Image Analysis*

The ADC maps were computed from the DWI results. The ADC maps were calculated pixel-by-pixel using ImageJ software (http://rsb.info.nih.gov/ij/, 1997–2012) using the following equation: ADC = −[ln(S/$S_0$)]/b, where S is the signal acquired (averaged over the 3 directions), b = 1000, and $S_0$ is the signal acquired without a diffusion gradient. The values were expressed in µm$^2$/s.

The standardized uptake value (SUV) (g/ml) maps were calculated as the measured tissue activity concentration (counts kBq/ml) divided by the injected activity in kBq per gram of body weight (kBq/g).

*Coregistration*

The ADC maps and FLAIR and $^{18}$FLT-PET images were coregistered with trilinear interpolation, rigid matching and normalized mutual information on 3DT1w-Gd images (PMOD 3.1® software) as described by Collet et al. [22].

*ROI Segmentation*

The region of T1 enhancement in the 3DT1w-Gd images was manually delineated, and the necrosis was excluded. The delineation proved difficult for 1 patient and the hypersignal in FLAIR images was considered.

For the ADC maps, the control ROI corresponded to the contralateral hemisphere following the manual exclusion of the CSF with pixels with values greater than 2000 µm$^2$/s. A manual correction was used when necessary.

The 5$^{th}$ percentile (5p) of ADC values were automatically thresholded and used to define the $ADC_{min}$, while the 95$^{th}$ percentile (95p) of SUV FLT values were defined as $FLT_{max}$. The 5$^{th}$ percentile cut-off value for ADC has already been used in various studies [28–31]. Although we used 90$^{th}$ percentile cut-off value for FLT in our previous study [22], we choose in the present study to use the 95$^{th}$ percentile by analogy to the 5$^{th}$ percentile of ADC.

*Parameter Extraction*

The tumor ROIs were reported on both the ADC and $^{18}$FLT-PET, to extract the mean and the maximum values for FLT, and the mean and the minimum value for the ADC.

The ROIs corresponding to the $ADC_{min}$ and $FLT_{max}$ were both reported on the modality of the ADC and FLT for calculating the respective mean values.

To evaluate the overlap between the ROI of $ADC_{min}$ and $FLT_{max}$, we added their binary threshold masks onto each other to calculate the Dice coefficient and to evaluate the overlap between these areas. Finally, these masks were added to the 3DT1w-Gd to visualize anatomic relationships.

*Statistical Analysis*

First, we evaluated the correlation between the $ADC_{min}$ (5p) and $FLT_{max}$ (95p) cut-off values using a linear regression test. Second, box-and-whisker plots were made between all the mean values of the different areas on the different modalities. A student's t-test was performed between the mean ADC values of the $ADC_{min}$ ROI and $FLT_{max}$ ROI and also between the mean FLT values of the $FLT_{max}$ ROI and $ADC_{min}$ ROI. Lastly, the mean value of the Dice coefficients was calculated.

## Results

The characteristics of the patient population and the $FLT_{max}$ SUV and $ADC_{min}$ cut-off values, along with the Dice coefficients, are shown in **Table 1**.

On anatomical MRI, all GBM were characterized by an extended peritumoral edema visible on the FLAIR. All patients also exhibited T1 enhancement area and necrosis was visible in almost all patients. In some cases, hemorrhages were also observed (but removed for the analysis).

As expected, all patients exhibited $^{18}$FLT uptake, as we already described in our previous paper by Collet et al. [22]. Of note, FLT was much more heterogeneous between patient but also within each tumor than anatomical MRI.

Both the ADC values and the FLT values were increased in the tumor region (the top line of **Fig. 1** for both patients), but a marked heterogeneity was also observed. No significant correlation between the $ADC_{min}$ and $FLT_{max}$ cut-off values was observed ($R^2$ = 0.0285, **Fig.2**).

The mean ADC values in the contralateral normal tissue (control), $ADC_{min}$ ROI and $FLT_{max}$ ROI, are shown in **Table 2** and graphically presented in **Fig. 3**. No significant difference was observed between the mean ADC values in the $ADC_{min}$ ROI and the values in the control ROI ($p$ = 0.79). However, the mean ADC values in the $FLT_{max}$-defined ROI (1130 ± 180 $\mu m^2/s$)

were significantly higher than the values in the $ADC_{min}$ ROI (808 ± 151 $\mu m^2/s$, $p < 0.001$) and the values in the control ROI (817 ± 51 $\mu m^2/s$, $p < 0.001$).

For FLT results, represented in **Table 2** and **Fig. 1**, mean values in the $FLT_{max}$ ROI (2.29 ± 0.92) were significantly higher than the values in the $ADC_{min}$ ROI (1.37 ± 0.63, $p < 0.001$).

Finally, we also analyzed the spatial correlation between the $ADC_{min}$ and $FLT_{max}$. Some representative slices of the 3DT1w-Gd, ADC, and $^{18}$FLT-PET maps with outlined maximum and minimum ROIs as overlaps for the ROI for two patients are shown in **Fig. 1**. Visually, we failed to show significant spatial overlap between the two ROIs. These results were confirmed with Dice coefficients, which also failed to show a significant overlap between the $ADC_{min}$ ROI and $FLT_{max}$ ROI (0.09 ± 0.11).

## Discussion

The major finding of our study is that we failed to show any correlation between the minimum ADC and maximum FLT. Our results are in agreement with those of the Rose et al. study [27], in which no correlation was observed between the minimum ADC and maximum FDOPA. Despite the presence of spatial overlap in some slices, it was reduced a lot when considering the whole tumor.

In line with our previous publication by Collet et al. [22], $^{18}$FLT uptake was observed in all patients. However, interestingly, a marker heterogeneity was observed with a range of $SUV_{max}$ from 0.71 to 3.95 g/ml. These results reinforce the value of metabolic imaging to go beyond anatomical MRI and to obtain more quantitative parameters.

The ADC is thought to reflect cellularity in cerebral tumors because of the reduced extracellular space [14]. One study that evaluated the relationship between the ADC and dynamic contrast-enhanced MRI measures of the volume of the extravascular extracellular space per unit volume ($v_e$) in patients with newly diagnosed gliomas reported that no correlation was found between the ADC and $v_e$ [32]. This study provides additional evidence that tumor regions with restrained diffusion do not necessarily correlate with regions with a reduced extracellular space. Although one study has shown a correlation between the ADC and Ki-67 in medulloblastomas [17], another one has shown no significant correlation between these two parameters in GBM [18]. More recently, in a study comparing the ability of various parameters extracted from multiparametric MRI that could predict Ki67 staining,

ADC maps was not a good predictor. Only a combination of variables with T2, fractional anisotropy, blood flow and permeability) gave accurate prediction of Ki67 staining [19].

Several explanations can be elaborated on the fact that this property of the ADC is no longer valid in the context of glioblastomas.

Rose et al. [27] evoked the presence of ischemia as a possible explanation for the lack of correlation between a low ADC and cellularity. In their results, they observed a reduced FDOPA uptake within regions of the minimum ADC (1.36 ± 0.22) compared with regions exhibiting a maximum FDOPA uptake (2.45 ± 0.88), which may be explained by the presence of ischemia, even though FDOPA PET is not a suitable exam for the evaluation of ischemia.

Even if we used a 1.5 T scanner in our study, the mean ADC in the normal brain tissue was 817 ± 51 $\mu m^2/s$ and the mean cutoff value was 808 ± 151 $\mu m^2/s$. This result strictly concurs with the results of Kang et al. [33], who reported a fifth percentile value of the ADC in high grade tumors of 782 ± 218 $\mu m^2/s$. However, the paper of Rose et al. used a minimum threshold of the ADC of 450 $\mu m^2/s$, which was calculated as being 3 SDs lower than the mean ADC values of normal parenchymal tissue. This value appears very low and is rather prerogative of cerebral infarction. Since ADC values result from a mathematical computation and are therefore independent of the magnetic field, the magnetic field is not at the origin of these differences as demonstrated in [34].

While ADC restriction has been proposed as a marker of GBM aggressivity, we observed in our results that $ADC_{min}$ was greater than the $ADC_{mean}$ of the contralateral cerebral tissue in 13 over 20 patients. This result concurs with previous studies showing increased ADC values in the GBM tumor. In one recent interesting study that aimed to determine and validate thresholds for the ADC values to distinguish GBM recurrence from pseudoprogression after standard treatment, a cut-off value of 1313 $\mu m^2/s$ was calculated with a sensitivity of 98.3% and specificity of 100.0% [35]. Altogether, these results reinforce the idea that ADC restriction is not a hallmark of GBM.

**Fig. 3** shows that, in addition to the lack of a significant difference in the mean ADC values between the normal tissue and $ADC_{min}$ ROI, the latter has a much wider range of values. This is mainly attributed to the well-known heterogeneous behavior of GBM. Hakyemez et al. [36] showed that the vast majority of GBM do not exhibit restricted diffusion in diffusion-weighted MRI, which is compatible with our results. This observation may be associated with edema, early stages of necrosis, liquefaction, and inflammatory

processes [36]. Indeed, GBM are heterogeneous by nature, both between different patients and within the tumor itself [37] and for this reason, we have chosen to use the fifth percentile method to calculate the minimum value of the ADC and the 95$^{th}$ percentile to calculate the maximum value of FLT for each patient. By this method, we consider this type of tumor an independent entity that will behave independently of the brain. In addition, this method provides almost identical volumes, so they are comparable, and the results will be pertinent. The choice of using the 5$^{th}$ percentile ADC rather than the true minimum ADC reduces the method's sensitivity to extreme aberrant values.

Another explanation of these results might be attributed to the methodology itself. The minimal ADC cut-off value (5p) considered could not be suitable for evaluating cellularity. This result obviously does not confirm the correlation between ADC and cellularity, even though authors relied in their discussion on the fact that the decreased diffusivity is the consequence of an enhanced tumor cell proliferation. This supports the idea that the ADC in the case of GBM should be calculated independently of the ADC in normal tissue. Two recent studies [38,39] also relied on the same hypothesis of the negative correlation between ADC and cellularity to demonstrate that a low ADC at the resection margin after resection surgery correlates with a poor chemoradiation response, overall survival [38] and infiltrative tumor load [39]. In any event, all these studies treated the ADC in peri-tumoral areas and not within the GBM, where behaviour can be very different.

Another important reason for the non-overlap between the minimal ADC and maximal FLT, or for the non-correlation between low ADC and cellularity in GBM, is tissue compression due to tumor growth. In our study, we minimized the impact of tumor growth between both imaging modalities by reducing the delay between the two examinations at 1 day. All the PET examinations were performed on Thursday and all of the MRI examinations on Friday. Lope-Piedrafita et al. [40] investigated the properties of water motion within and around brain tumors as a function of tumor growth in an animal glioma model, and they reported a reduced ADC in the tissue immediately surrounding the growing tumor. This finding was explained by the change in the shape of the cells in the immediate vicinity of tumor growth. The ROI of the fifth percentile of the ADC being mainly distributed in the periphery of our tumor mask was constantly observed in our study, as shown in **Fig. 4**.

Other various processes were also discussed in many studies to explain the restriction of diffusion inside of tumor cavity, such as intratumoral hemorrhage, cytotoxic

edema at the early phase of cell death, thick sterile liquefaction and pyogenic infection [41–46].

In our study, large hemorrhages were removed and regarding our mean ADC values, hugged restrictions were not observed suggesting that the impact of these parameters was not predominant in our results.

## Conclusions

As a conclusion, no significant correlation between the minimum ADC and maximum FLT was observed nor any significant anatomical overlap between the low ADC and high FLT. While $^{18}$FLT-PET provides further information than $^{18}$FDG-PET to go further glucose metabolism by enabling tumor cell proliferation, our result raises the question about the reliability to use ADC as an index of cellular proliferation, and the role of ADC maps in GBM is yet to be elaborated. ADC may rather reflect edema, early stages of necrosis, liquefaction, and inflammatory processes. Interestingly, the present study reinforces the interest of multimodal imaging to deeply characterize glioblastoma.

## Funding

This study was funded by the Institut National contre le Cancer (INCa), the Conseil Régional de Basse-Normandie (CRBN), the European Union – « Fonds Européen de Développement Régional (FEDER) », l'Europe s'engage en Basse-Normandie and the French National Agency for Research called "Investissements d'Avenir" no. ANR-11-LABEX-0018-01.

## Conflict of interest

The authors declare that they have no conflict of interest.

## References


[1] Bartek J, Ng K, Bartek J, Fischer W, Carter B, Chen CC. Key concepts in glioblastoma therapy. J Neurol Neurosurg Psychiatry 2012;83:753–60.

[2] Lacroix M, Abi-Said D, Fourney DR, Gokaslan ZL, Shi W, DeMonte F, et al. A multivariate analysis of 416 patients with glioblastoma multiforme: prognosis, extent of resection, and survival. J Neurosurg 2001;95:190–8.

[3] Tait MJ, Petrik V, Loosemore A, Bell BA, Papadopoulos MC. Survival of patients with glioblastoma multiforme has not improved between 1993 and 2004: analysis of 625 cases. Br J Neurosurg 2007;21:496–500.

[4] Kono K, Inoue Y, Nakayama K, Shakudo M, Morino M, Ohata K, et al. The role of diffusion-weighted imaging in patients with brain tumors. AJNR Am J Neuroradiol 2001;22:1081–8.

[5] Chien D, Buxton RB, Kwong KK, Brady TJ, Rosen BR. MR diffusion imaging of the human brain. J Comput Assist Tomogr n.d.;14:514–20.

[6] Flacke S, Urbach H, Folkers PJ, Keller E, van den Brink JS, Träber F, et al. Ultra-fast three-dimensional MR perfusion imaging of the entire brain in acute stroke assessment. J Magn Reson Imaging 2000;11:250–9.

[7] Tschampa HJ, Mürtz P, Flacke S, Paus S, Schild HH, Urbach H. Thalamic involvement in sporadic Creutzfeldt-Jakob disease: a diffusion-weighted MR imaging study. AJNR Am J Neuroradiol 2003;24:908–15.

[8] Le Bihan D, Breton E, Lallemand D, Grenier P, Cabanis E, Laval-Jeantet M. MR imaging of intravoxel incoherent motions: application to diffusion and perfusion in neurologic disorders. Radiology 1986;161:401–7.

[9] Tien RD, Felsberg GJ, Friedman H, Brown M, MacFall J. MR imaging of high-grade cerebral gliomas: value of diffusion-weighted echoplanar pulse sequences. AJR Am J Roentgenol 1994;162:671–7.

[10] Guzman R, Altrichter S, El-Koussy M, Gralla J, Weis J, Barth A, et al. Contribution of the apparent diffusion coefficient in perilesional edema for the assessment of brain tumors. J Neuroradiol 2008;35:224–9.

[11] Stadnik TW, Chaskis C, Michotte A, Shabana WM, van Rompaey K, Luypaert R, et al. Diffusion-weighted MR imaging of intracerebral masses: comparison with conventional MR imaging and histologic findings. AJNR Am J Neuroradiol

2001;22:969–76.

[12] Castillo M, Smith JK, Kwock L, Wilber K. Apparent diffusion coefficients in the evaluation of high-grade cerebral gliomas. AJNR Am J Neuroradiol 2001;22:60–4.

[13] Pauleit D, Langen K-J, Floeth F, Hautzel H, Riemenschneider MJ, Reifenberger G, et al. Can the apparent diffusion coefficient be used as a noninvasive parameter to distinguish tumor tissue from peritumoral tissue in cerebral gliomas? J Magn Reson Imaging 2004;20:758–64.

[14] Cha S. Update on brain tumor imaging: from anatomy to physiology. AJNR Am J Neuroradiol 2006;27:475–87.

[15] Sugahara T, Korogi Y, Kochi M, Ikushima I, Shigematu Y, Hirai T, et al. Usefulness of diffusion-weighted MRI with echo-planar technique in the evaluation of cellularity in gliomas. J Magn Reson Imaging 1999;9:53–60.

[16] Kitis O, Altay H, Calli C, Yunten N, Akalin T, Yurtseven T. Minimum apparent diffusion coefficients in the evaluation of brain tumors. Eur J Radiol 2005;55:393–400.

[17] Yamashita Y, Kumabe T, Higano S, Watanabe M, Tominaga T. Minimum apparent diffusion coefficient is significantly correlated with cellularity in medulloblastomas. Neurol Res 2009;31:940–6.

[18] Higano S, Yun X, Kumabe T, Watanabe M, Mugikura S, Umetsu A, et al. Malignant astrocytic tumors: clinical importance of apparent diffusion coefficient in prediction of grade and prognosis. Radiology 2006;241:839–46.

[19] Gates EDH, Lin JS, Weinberg JS, Hamilton J, Prabhu SS, Hazle JD, et al. Guiding the First Biopsy in glioma patients using estimated Ki67 maps derived from magnetic resonance imaging: conventional versus advanced imaging. Neuro Oncol 2019.

[20] Rasey JS, Grierson JR, Wiens LW, Kolb PD, Schwartz JL. Validation of FLT uptake as a measure of thymidine kinase-1 activity in A549 carcinoma cells. J Nucl Med 2002;43:1210–7.

[21] Chalkidou A, Landau DB, Odell EW, Cornelius VR, O'Doherty MJ, Marsden PK. Correlation between Ki-67 immunohistochemistry and 18F-fluorothymidine uptake in patients with cancer: A systematic review and meta-analysis. Eur J Cancer 2012;48:3499–513.

[22] Collet S, Valable S, Constans JM, Lechapt-Zalcman E, Roussel S, Delcroix N, et al. [18F]-fluoro-l-thymidine PET and advanced MRI for preoperative grading of gliomas.

NeuroImage Clin 2015;8:448–54.

[23] Chen W, Cloughesy T, Kamdar N, Satyamurthy N, Bergsneider M, Liau L, et al. Imaging proliferation in brain tumors with 18F-FLT PET: comparison with 18F-FDG. J Nucl Med 2005;46:945–52.

[24] Hatakeyama T, Kawai N, Nishiyama Y, Yamamoto Y, Sasakawa Y, Ichikawa T, et al. 11C-methionine (MET) and 18F-fluorothymidine (FLT) PET in patients with newly diagnosed glioma. Eur J Nucl Med Mol Imaging 2008;35:2009–17.

[25] Jacobs AH, Thomas A, Kracht LW, Li H, Dittmar C, Garlip G, et al. 18F-fluoro-L-thymidine and 11C-methylmethionine as markers of increased transport and proliferation in brain tumors. J Nucl Med 2005;46:1948–58.

[26] Zukotynski KA, Vajapeyam S, Fahey FH, Kocak M, Brown D, Ricci KI, et al. Correlation of 18 F-FDG PET and MRI Apparent Diffusion Coefficient Histogram Metrics with Survival in Diffuse Intrinsic Pontine Glioma: A Report from the Pediatric Brain Tumor Consortium. J Nucl Med 2017;58:1264–9.

[27] Rose S, Fay M, Thomas P, Bourgeat P, Dowson N, Salvado O, et al. Correlation of MRI-derived apparent diffusion coefficients in newly diagnosed gliomas with [18F]-fluoro-L-dopa PET: what are we really measuring with minimum ADC? AJNR Am J Neuroradiol 2013;34:758–64.

[28] Hong EK, Choi SH, Shin DJ, Jo SW, Yoo R-E, Kang KM, et al. Radiogenomics correlation between MR imaging features and major genetic profiles in glioblastoma. Eur Radiol 2018;28:4350–61.

[29] Zhang Y, Zhang Q, Wang X -x., Deng X -f., Zhu Y -z. Value of pretherapeutic DWI in evaluating prognosis and therapeutic effect in immunocompetent patients with primary central nervous system lymphoma given high-dose methotrexate-based chemotherapy: ADC-based assessment. Clin Radiol 2016;71:1018–29.

[30] Zhang M, Gulotta B, Thomas A, Kaley T, Karimi S, Gavrilovic I, et al. Large-volume low apparent diffusion coefficient lesions predict poor survival in bevacizumab-treated glioblastoma patients. Neuro Oncol 2016;18:735–43.

[31] Kralik SF, Taha A, Kamer AP, Cardinal JS, Seltman TA, Ho CY. Diffusion imaging for tumor grading of supratentorial brain tumors in the first year of life. Am J Neuroradiol 2014;35:815–23.

[32] Mills SJ, Soh C, Rose CJ, Cheung S, Zhao S, Parker GJM, et al. Candidate biomarkers of

extravascular extracellular space: a direct comparison of apparent diffusion coefficient and dynamic contrast-enhanced MR imaging-derived measurement of the volume of the extravascular extracellular space in glioblastoma multiforme. AJNR Am J Neuroradiol 2010;31:549-53.

[33] Kang Y, Choi SH, Kim Y-J, Kim KG, Sohn C-H, Kim J-H, et al. Gliomas: Histogram analysis of apparent diffusion coefficient maps with standard- or high- b -value diffusion-weighted MR imaging—correlation with tumor grade. Radiology 2011;261:882–90.

[34] Merhemic Z, Imsirovic B, Bilalovic N, Stojanov D, Boban J, Thurnher MM. Apparent diffusion coefficient reproducibility in brain tumors measured on 1.5 and 3 T clinical scanners: A pilot study. Eur J Radiol 2018;108:249–53.

[35] Kazda T, Bulik M, Pospisil P, Lakomy R, Smrcka M, Slampa P, et al. Advanced MRI increases the diagnostic accuracy of recurrent glioblastoma: Single institution thresholds and validation of MR spectroscopy and diffusion weighted MR imaging. NeuroImage Clin 2016;11:316–21.

[36] Hakyemez B, Erdogan C, Yildirim N, Parlak M. Glioblastoma multiforme with atypical diffusion-weighted MR findings. Br J Radiol 2005;78:989–92.

[37] Aum DJ, Kim DH, Beaumont TL, Leuthardt EC, Dunn GP, Kim AH. Molecular and cellular heterogeneity: the hallmark of glioblastoma. Neurosurg Focus 2014;37:E11.

[38] Qu J, Qin L, Cheng S, Leung K, Li X, Li H, et al. Residual low ADC and high FA at the resection margin correlate with poor chemoradiation response and overall survival in high-grade glioma patients. Eur J Radiol 2016;85:657–64.

[39] van der Hoorn A, Yan J-L, Larkin TJ, Boonzaier NR, Matys T, Price SJ. Posttreatment apparent diffusion coefficient changes in the periresectional area in patients with glioblastoma. World Neurosurg 2016;92:159–65.

[40] Lope-Piedrafita S, Garcia-Martin ML, Galons J-P, Gillies RJ, Trouard TP. Longitudinal diffusion tensor imaging in a rat brain glioma model. NMR Biomed 2008;21:799-808.

[41] Holtås S, Geijer B, Strömblad LG, Maly-Sundgren P, Burtscher IM. A ring-enhancing metastasis with central high signal on diffusion-weighted imaging and low apparent diffusion coefficients. Neuroradiology 2000;42:824–7.

[42] Tung GA, Evangelista P, Rogg JM, Duncan JA. Diffusion-weighted MR imaging of rim-enhancing brain masses: is markedly decreased water diffusion specific for brain abscess? AJR Am J Roentgenol 2001;177:709–12.

[43] Batra A, Tripathi RP. Atypical diffusion-weighted magnetic resonance findings in glioblastoma multiforme. Australas Radiol 2004;48:388–91.

[44] Dorenbeck U, Butz B, Schlaier J, Bretschneider T, Schuierer G, Feuerbach S. Diffusion-weighted echo-planar MRI of the brain with calculated ADCs: a useful tool in the differential diagnosis of tumor necrosis from abscess? J Neuroimaging 2003;13:330–8.

[45] Mori H, Abe O, Aoki S, Masumoto T, Yoshikawa T, Kunimatsu A, et al. Hemorrhagic brain metastases with high signal intensity on diffusion-weighted MR images. A case report. Acta Radiol 2002;43:563–6.

[46] Park SH, Chang KH, Song IC, Kim YJ, Kim SH, Han MH. Diffusion-weighted MRI in cystic or necrotic intracranial lesions. Neuroradiology 2000;42:716–21.

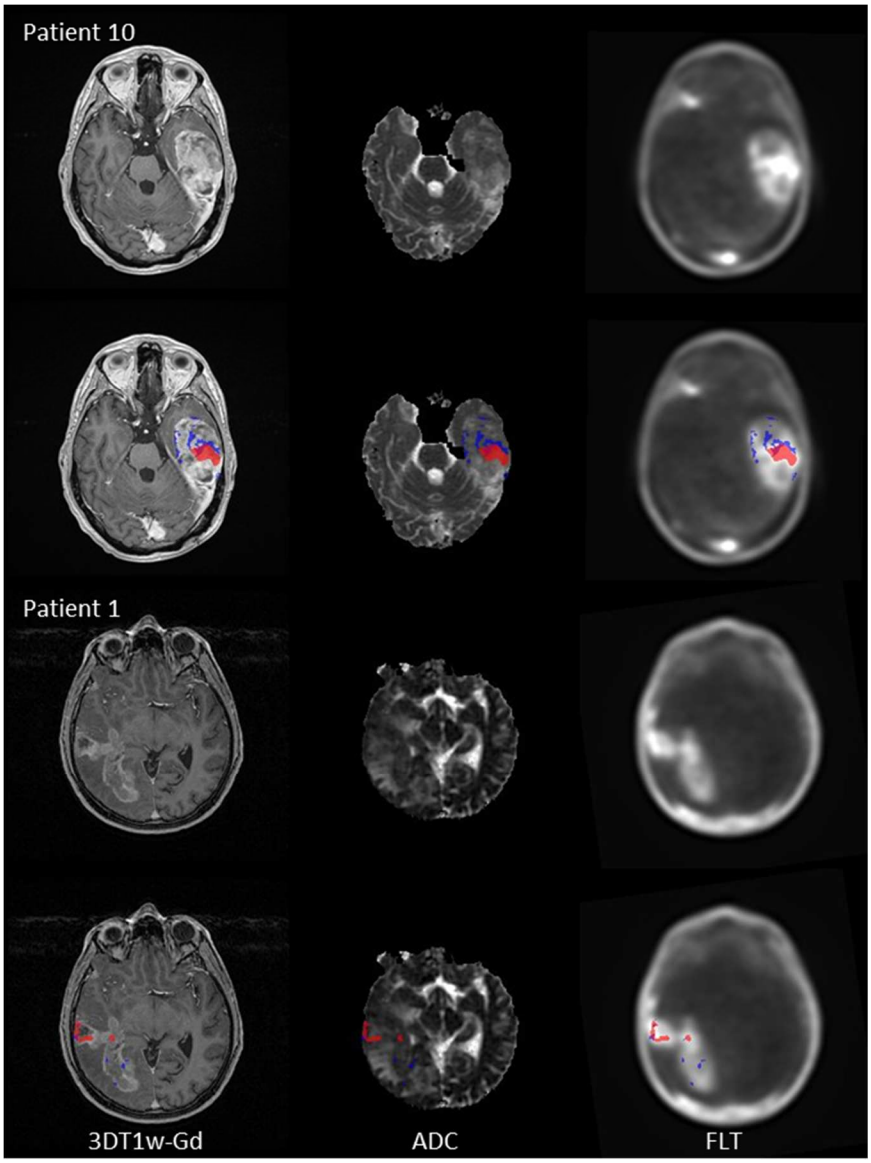



**Fig. 1.** Illustrative slices of registered 3DT1w-Gd, ADC and FLT images, for two patients. For each patient, images are represented without (top) and with (bottom) overlays. The blue overlay is for $ADC_{min}$ ROI and the red overlay is for $FLT_{max}$ ROI. Patient 10 had a considerable overlap, but the overlap between these 2 regions in Patient 1 was almost null.

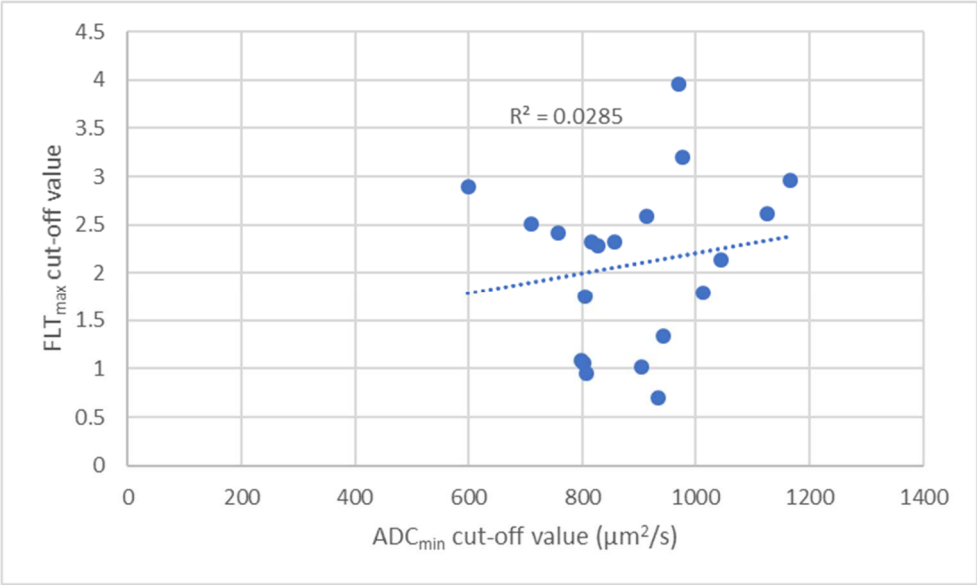



**Fig. 2.** Scatterplot with linear regression line illustrating the relationship between the cut-off values of $ADC_{min}$ and $FLT_{max}$. No significant correlation was found.

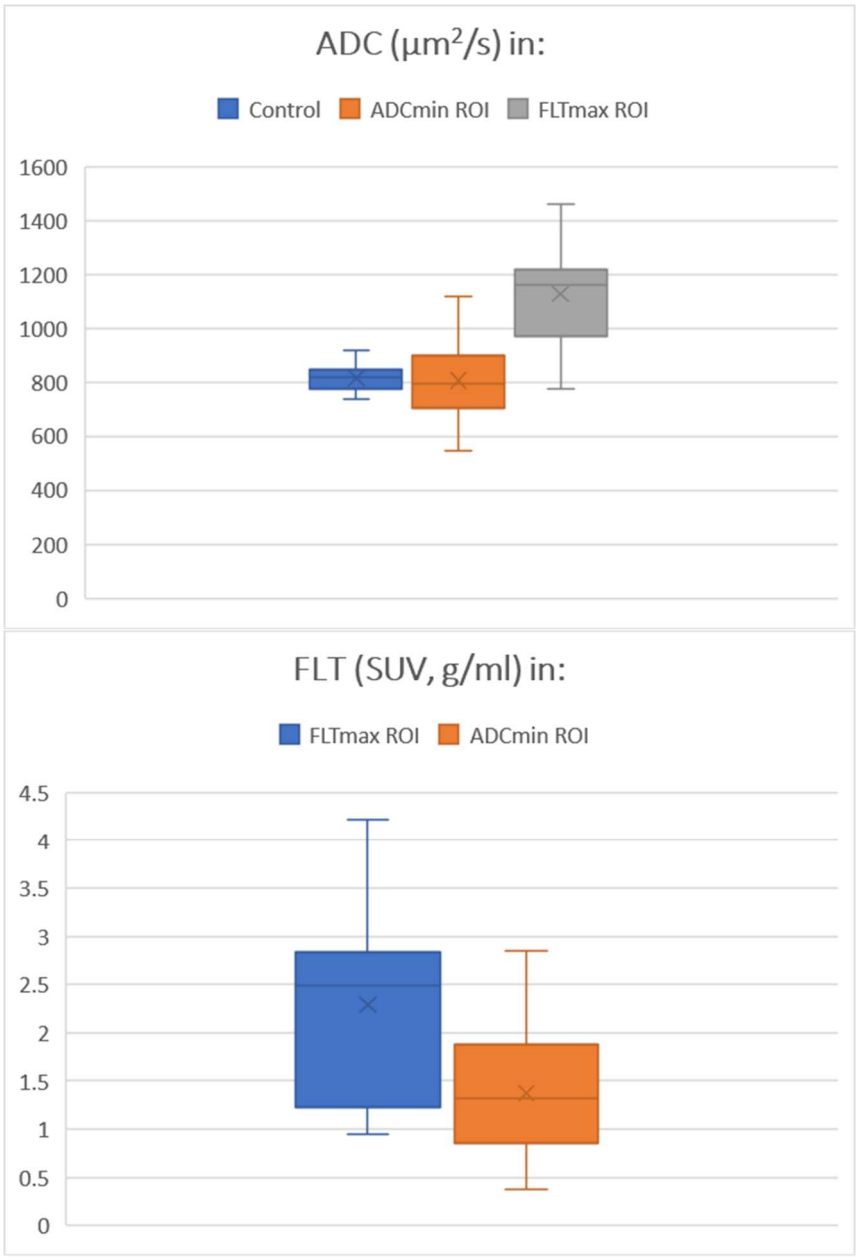



**Fig. 3.** Box-and-whisker plots outlining the distribution (mean and SD) of ADC and FLT in control, $ADC_{min}$ and $FLT_{max}$ ROIs.

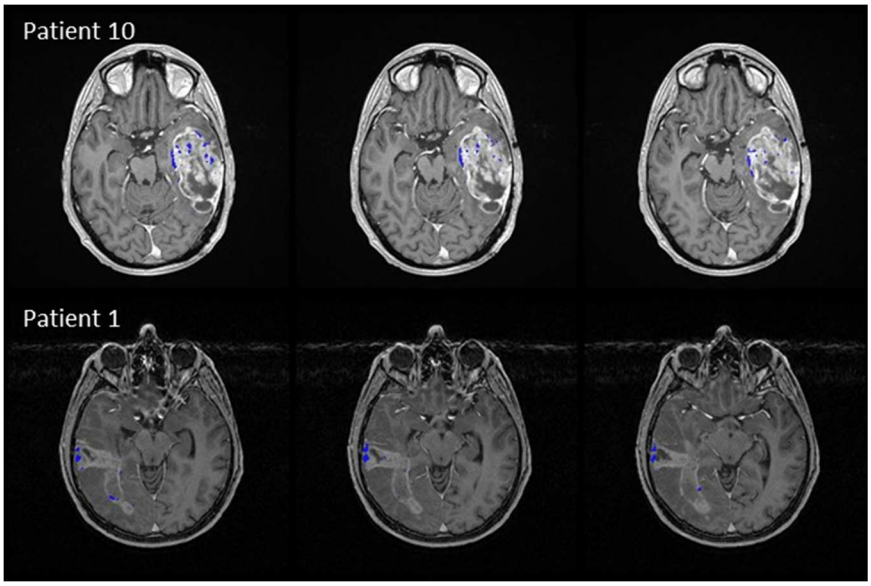



**Fig. 4.** Serial representative slices of 3DT1w-Gd images with the corresponding $ADC_{min}$ ROI (blue overlay). We observe that most of this ROI is distributed around the outermost border of the tumor.

**Table 1**

The patient demographics, minimum ADC ($ADC_{min}$) and maximum FLT ($FLT_{max}$) cut-off values, and Dice indices.

| Patient | Sex/Age (yr) | Cut-off Value | | Dice |
|---|---|---|---|---|
| | | $ADC_{min}$[a] | $FLT_{max}$ | |
| 1 | M/58 | 808 | 0.96 | 0.12 |
| 2 | F/74 | 913 | 2.59 | 0.04 |
| 3 | M/73 | 976 | 3.19 | 0.05 |
| 4 | M/59 | 1044 | 2.13 | 0 |
| 5 | M/70 | 804 | 1.06 | 0.32 |
| 6 | F/44 | 599 | 2.9 | 0.01 |
| 7 | F/46 | 1127 | 2.61 | 0 |
| 8 | M/52 | 758 | 2.41 | 0.16 |
| 9 | F/70 | 799 | 1.08 | 0.01 |
| 10 | M/28 | 1012 | 1.79 | 0.15 |
| 11 | M/58 | 970 | 3.95 | 0.03 |
| 12 | M/79 | 857 | 2.32 | 0.4 |
| 13 | M/67 | 943 | 1.33 | 0.06 |
| 14 | M/53 | 1167 | 2.96 | 0.25 |
| 15 | F/38 | 934 | 0.71 | 0.01 |
| 16 | M/64 | 817 | 2.32 | 0.01 |
| 17 | M/52 | 805 | 1.75 | 0 |
| 18 | M/74 | 905 | 1.02 | 0.05 |
| 19 | M/62 | 710 | 2.5 | 0 |
| 20 | M/67 | 828 | 2.29 | 0.07 |
| Mean (SD) | | 889 (139) | 2.09 (0.87) | 0.09 (0.12) |

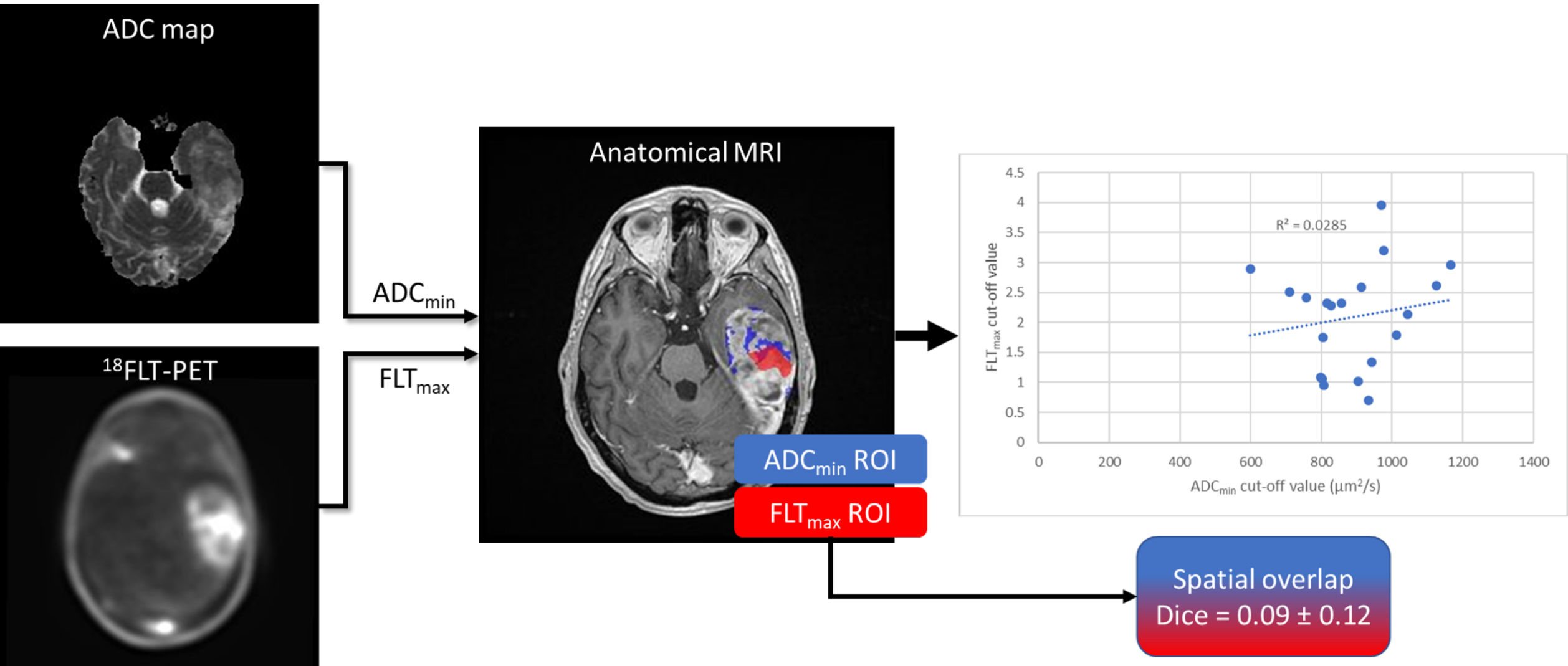
[a] $\mu m^2/s$

**Table 2**

The mean ADC values in the control, $ADC_{min}$, and $FLT_{max}$ ROIs and the mean FLT values in the $FLT_{max}$ and $ADC_{min}$ ROIs. * *p<0.001* vs. the control region; # *p<0.001* vs. the $ADC_{min}$ ROI; $ *p<0.001* vs. the $FLT_{max}$ ROI.

| | ADC value[a, b] | | | FLT value[b] | |
|---|---|---|---|---|---|
| Patient | Control | $ADC_{min}$ ROI | $FLT_{max}$ ROI | $FLT_{max}$ ROI | $ADC_{min}$ ROI |
| 1 | 741 (100) | 766 (40) | 963 (136) | 1.04 (0.06) | 0.58 (0.23) |
| 2 | 851 (154) | 766 (236) | 1098 (179) | 2.75 (0.12) | 1.34 (0.63) |
| 3 | 884 (186) | 917 (68) | 1189 (139) | 3.43 (0.22) | 1.95 (0.69) |
| 4 | 754 (122) | 979 (55) | 1459 (134) | 2.29 (0.11) | 1.32 (0.23) |
| 5 | 912 (213) | 764 (30) | 890 (123) | 1.11 (0.03) | 0.95 (0.19) |
| 6 | 786 (115) | 552 (38) | 776 (92) | 3.21 (0.24) | 1.6 (0.54) |
| 7 | 792 (98) | 1050 (71) | 1432 (142) | 2.84 (0.15) | 1.01 (0.4) |
| 8 | 742 (74) | 691 (59) | 999 (256) | 2.62 (0.16) | 2.04 (0.4) |
| 9 | 822 (107) | 725 (69) | 1173 (238) | 1.14 (0.04) | 0.62 (0.23) |
| 10 | 841 (127) | 883 (195) | 1189 (304) | 2.29 (0.49) | 1.32 (0.63) |
| 11 | 774 (112) | 905 (62) | 1152 (99) | 4.22 (0.24) | 2.85 (0.69) |
| 12 | 919 (177) | 796 (44) | 942 (196) | 2.82 (0.38) | 2.09 (0.87) |
| 13 | 771 (81) | 889 (51) | 1176 (206) | 1.49 (0.14) | 0.82 (0.28) |
| 14 | 816 (127) | 1120 (41) | 1297 (179) | 3.11 (0.1) | 2.26 (0.72) |
| 15 | 803 (79) | 860 (83) | 1355 (295) | 0.95 (0.24) | 0.38 (0.13) |
| 16 | 789 (117) | 547 (215) | 1228 (169) | 2.49 (0.12) | 1.32 (0.39) |
| 17 | 823(103) | 703 (97) | 1035 (149) | 1.86 (0.09) | 1.21 (0.24) |
| 18 | 837 (128) | 845 (47) | 1191 (221) | 1.07 (0.05) | 0.73 (0.2) |
| 19 | 854 (124) | 603 (111) | 1115 (161) | 2.63 (0.11) | 1.65 (0.31) |
| 20 | 838 (93) | 799 (26) | 936 (101) | 2.48 (0.16) | 1.44 (0.56) |
| Mean (SD) | 817 (51) | 808 (151) | 1130 (180) *; # | 2.29 (0.92) | 1.37 (0.63) $ |

[a] $\mu m^2/s$; [b] mean (SD) values.


ADC map
$^{18}$FLT-PET
$ADC_{min}$
$FLT_{max}$
Anatomical MRI
$ADC_{min}$ ROI
$FLT_{max}$ ROI
Spatial overlap
Dice = 0.09 ± 0.12
$R^2$ = 0.0285
$FLT_{max}$ cut-off value
$ADC_{min}$ cut-off value (µm²/s)
0
0.5
1
1.5
2
2.5
3
3.5
4
4.5
0
200
400
600
800
1000
1200
1400